Jurnal Kejuruteraan 31(2) 2019: 249-259
https://doi.org/10.17576/jkukm-2019-31(2)-09

The Load Performance of Multi-Level Alternating Voltage Provided by Upgrade Effect

Erol CAN
School of Civil Aviation, Erzincan University, Aircraft Airframe Power Plant, Erzincan, Turkey
**Corresponding author: can_e@hotmail.com*

Received 14 January 2019, Received in revised form 14 March 2019
Accepted 17 March 2019, Available online 31 October 2019

ABSTRACT

In this paper, the applications of the multi-level inverter with a partial inductor are investigated on different loads. The operation of the inverter is given according to different conditions of the circuit at the six-part duty times. Mathematical equations for the inverter are forming according to the load which is resistive (R), inductive (L), and Capacitive (C) in serial connection. After describing the circuit structure, Matlab SIMULİNK also simulates the circuit for loads that are RLC, and a single-phase asynchronous motor. While the voltage and current measurements for the RLC load are performed; measurements of the main winding current, auxiliary winding current, electromagnetic torque, speed are made on the asynchronous motor. RLC loads are operated at high current values such as 297A in order to examine the suitability of the proposed system for systems that may require high current. When the current harmonic distortions of RLC loads are observed, the distortion values are acceptable values that are lower than % 5 that is international standards of the IEEE. In another hand, despite the voltage is insufficient for supplying the motor at the motor application, the voltage is upgraded with the boost effect of the inverter. So, the voltage is both a multilevel and sufficient. According to the obtained results, it is shown that multi-level inverter design has been successfully performed by using partial inductor source.

Keywords: Partial inductor source; different working times; the upgrade effect of the inverter

INTRODUCTION

It is desirable to convert the DC power source into an alternating energy source according to the intended use and the production conditions (Breyer et al. 2018; Harun 2017 et al.; Viana et al. 2018; Singh et al. 2017; Yusof et al. 2011). Thus, many single-phase and multi-phase inverters have been used in the literature **(**Singh et al. 2018; Can & Sayan 2016; Reddy et al. 2017; Can 2017; Babae 2018). If an alternating voltage is to obtain on the load at a level higher than the applied DC input voltage (Ahmadi & Aleenejad 2019; Cavalcanti et al. 2018; Madhu et al. 2018), it is preferable to operate the Z source inverter. On the other hand, multi-level inverters are only used to generate multiple levels of voltage. In this study, the application of a multi-level inverter with the partial sources is presented. The inverter provides a higher alternating voltage at the maximum value according to the maximum value of an input DC voltage at the load when it creates multi-level voltage. While conventional Z source inverters are increasing the entire voltage on the load, the proposed inverter uses firstly this effect to generate a multilevel voltage. Therefore, with the proposed inverter method, the voltage value increases while the multi-level voltage occurs. The proposed circuit has an upgrade effect except that it generates multiple levels, while conventional multi-level inverter structures focus only on generating voltage levels. To create this circuit, 12 IGBT switches are controlled with six-piece Linear Pulse Width Modulation (PWM). Multi-level voltage is obtained on the four different circuit states obtained with these six PWMs. After design and mathematical equations are created according to the RLC load in serial connection according to the four different circuit states obtained, mathematical equations are created for the simulation model of the single-phase asynchronous motor. At the application, the proposed model is tried at the Matlab Simulink. Firstly, Resistive (R), Inductive (L) and, (C) capacitive loads connected in series are operated for 10-50 micro-Henry of source inductor value. For this source condition, the load voltage and currents are measured. The load current harmonic distortion is investigated in order to show the alternating current produced within the quality standards and acceptable. Therefore, the distortion values compare with the standard of international IEEE. According to the obtained results, the alternating currents produced are in quality standards while the currents achieve full sinus shape. Secondly, the single-phase asynchronous motor is tried with the capacitor-start mode at Matlab Simulink after the mathematical model of single-phase asynchronous motor is described. Although many motor driving applications have been made by the inverter so far, the proposed method differs from the other studies with the different method of producing multi-level voltage on the motor windings (Huang et al. 2018; Singh et al. 2018; Rajesh 2018). The inverter uses the same voltage source for each level of voltage in the motor windings. However, there are inductors which are connected in series to the sources that will generate the high-level voltage. These

inductors provide a high level at the center of voltage on the motor windings. It is aimed to create a higher alternating voltage on the motor windings according to the maximum level of the voltage values of the available sources that are not enough to run the motor in full performance. Although this is not the case for multi-level alternating voltage generated with the effect of the increases in other inverter and motor driving applications, this study demonstrates the motor drive with multi-level alternating voltage generated with the effect of the increases (Kim & Balog 2018; Nguyen et al. 2018; Singh et al. 2018; Yao et al. 2018; Kumar 2018; Ananda 2018; Paterakis 2018). After the simulation applications; the stabilization of the main winding current and the stabilization of the auxiliary winding current of the motor are investigated at time axis. The motor can be used for the full performance although the motor is supplied with a voltage that is less than the required voltage. For testing the effect of the inductor on the circuit; the inverter has a unilateral inductor source while the motor is driven. For engine performance, the speed, torque, main and auxiliary winding current values are observed if this is to show the effect of the fragmented source in the proposed system. According to the results obtained, it is observed that the single phase induction motor is driven successfully.

MULTI-LEVEL INVERTOR STRUCTURE WITH PARTS INDUCTION

Figure 1a shows the proposed inverter circuit, while figure 1b shows the operating angles of the switches and the PWMs operating these switches. The inverter circuit in Figure 1 also includes S0 to S11 twelve IGBT switches, D0-D1 two diodes, V0 to V3 four equal voltage sources, L2-L3 equal two inductors for sources. R, L, C is load in serial connection.

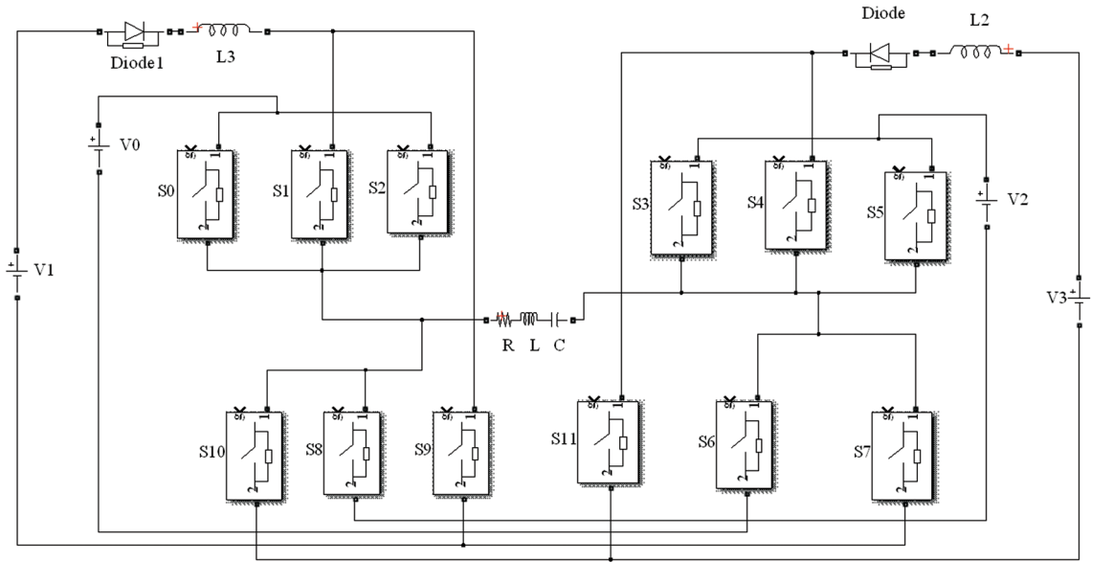

(a)

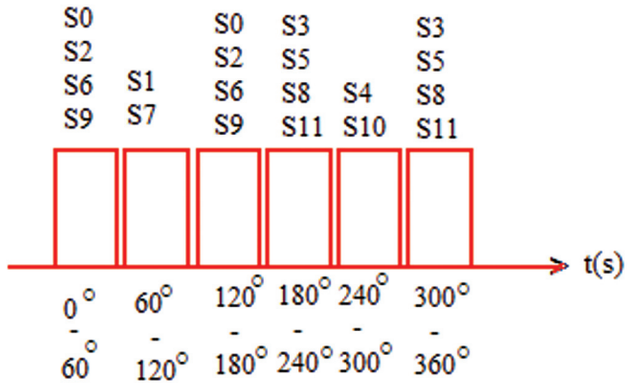

(b)

FIGURE 1. (a) Multi-level inverter with single-phase partial inductor, (b) PWMs

In the circuit in Figure 1, four-level alternating voltage of 360 degrees is formed in six steps. The switches and circuit structure to be operated for voltage at 0°-60° and 120°-180° of electrical angles for the first level of alternating voltage positive side are given in Figure 2. The elements working of the system in these electrical angles are specified at the figure, while the non-working elements are made of transparent at the figures.

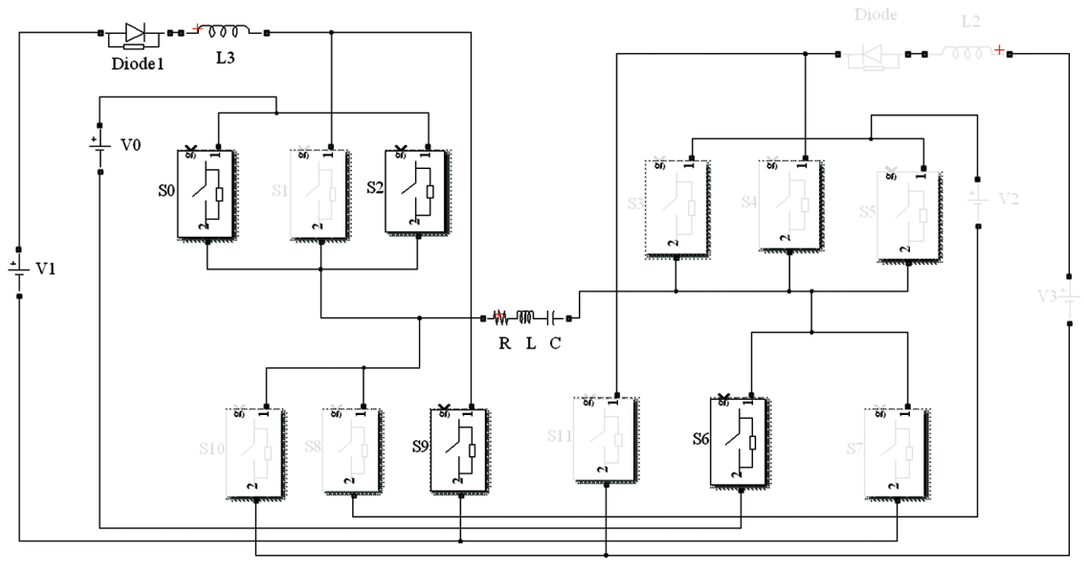

FIGURE 2. Circuit elements working to produce voltage at 0°-60° and 120°-180° of electrical angles

In order to generate the first level voltage on the positive side, the switches S0, S2, S6 in electrical angles of 0°-60° and 120°-180° operate the V0 source on the load. In these angles, the L3 inductor is stored from the V1 source. The voltage on the load is calculated as in Eq.1. i_1 is the current generated by the voltage at 0° to 60° degrees of electrical angles; i_2 is the current generated by the voltage at 120°-180° degrees. $i_1 = i_2$.

$$U_{60}^{0} = U_{180}^{0} = (di_1/dt)L + R*i_{1+}\, i_1/C \quad (1)$$

For the L3 of inductor is stored with current flowing through the V1 source at this level, Eq. 2 can be written. i_{d1} is the value of the stored current, the voltage generated is U_{d1} when the current is being stored.

$$U_{d1} = (di_{d1}/dt)L3 \quad (2)$$

In Figure 3, the elements D1, L3, S1, S7 operate the source DCV1 on the load at an electrical angle of 60°-120° to generate the second level voltage on the positive side.

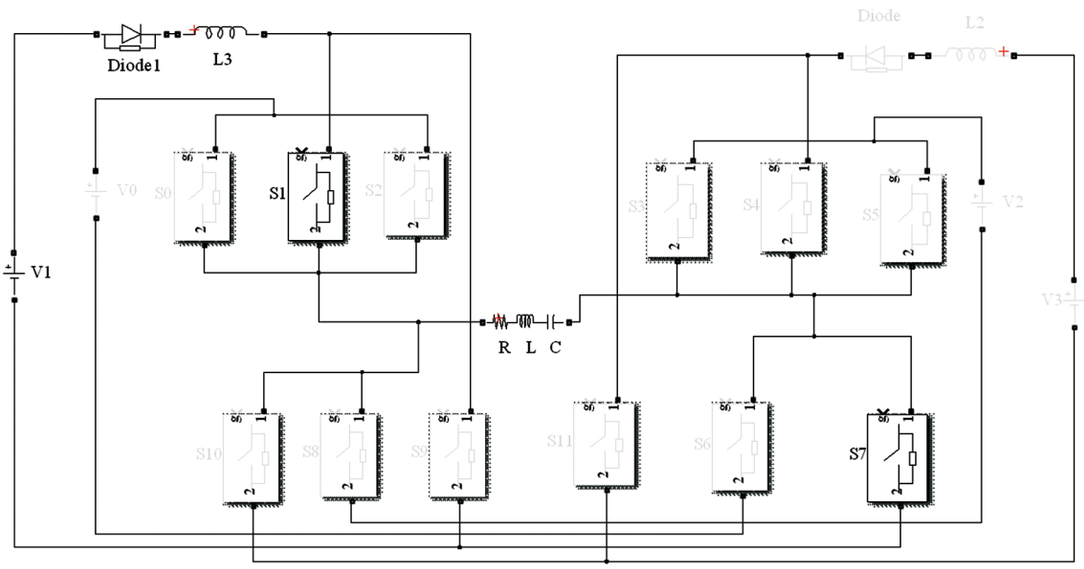

FIGURE 3. Circuit elements operating at 60-120 voltage to produce voltage

The voltage $U_{120}{}^{0}$, which will create the high level on the positive side of the voltage, can be described as Eq. 3. i_3 and d_{i3} are the external current values than the current stored by the inductor at 60°-120° of electrical angle.

$$U_{120}{}^{0} = (di_3/dt)(L1 + L3) + (di_{d1}/dt)L3 + R*i_{3+}i_3/C \quad (3)$$

Switches and circuit structure to be operated for voltage at 180-240 and 300-360 degrees are given in Figure 4.

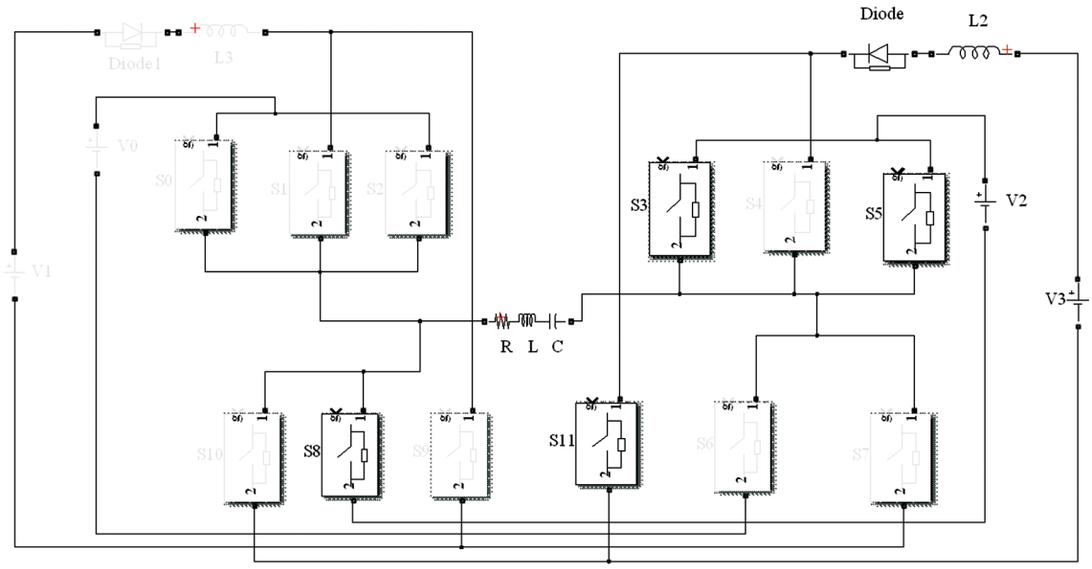

FIGURE 4. Operating circuit elements to produce the voltage at degrees 180-240 and 300-360 of elctrical angle

In order to generate the first level voltage on the negative side, the switches S3, S5, S8 in electrical angles 180-240 and 300-360 operate the V2 source on the load. In these angles, the L_2 coil is stored from the V3 source. The voltage on the load is similar to that of Eq. 4. i_4 is the current generated by the voltage at 0 to 60 degrees; i_5 is the current generated by the voltage at 120-180 degrees. $I_4 = i_5$.

$$U_{240}{}^{0} = U_{360}{}^{0} = (di_4/dt)L1 + R*i_{4+}i_4/C \quad (4)$$

For the L2 of inductor is stored with current flowing through the V3 source at this level, Eq. 5 can be written. i_{d2} is the value of the stored current, the voltage generated is U_{d2} when the current is being stored.

$$U_{d2} = (di_{d2}/dt)L3 \quad (5)$$

The elements D0, L2, S4, S10 in Figure 5 operate the source V3 on the load at an electrical angle of 240°-300° in order to generate the second level voltage on positive side of the alternating voltage.

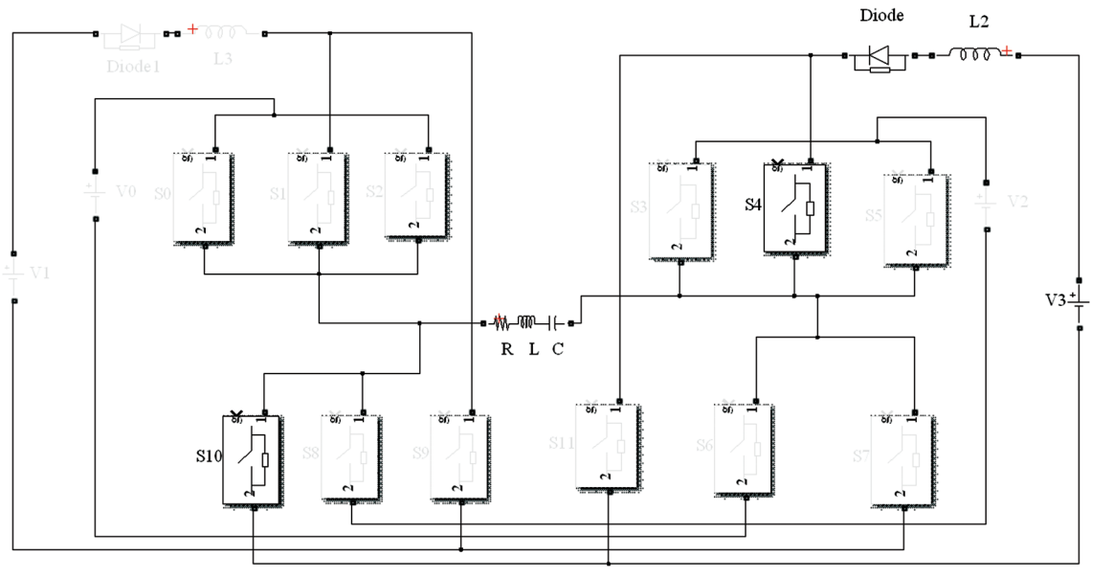

FIGURE 5. Circuit elements to produce voltage at 240-300 electrical angles

The U_{240}^{0} voltage, which creates the high level on the positive side of the voltage, can be defined as Eq. 6. i_6 and di6 external current values are from stored by the inductor at 240-300 degrees.

$$U_{240}^{0} = (di_6/dt)(L1 + L2) + (di_{d2}/dt)L2 + R*i_6 + i_6/C \quad (6)$$

In this study, the proposed circuit structure is also applied in single-phase asynchronous motor application.

Single phase asynchronous motor is operated as capacitor start mode. The connection of the capacitor to the motor windings is given in figure 6 in asynchronous motors with one-phase capacitors; a capacitor is connected in series to the auxiliary winding so that the current flowing through the auxiliary winding is at a forward electrical angle according to electrical angle of the voltage. Thus, a phase difference of 90 degrees occurs between the main and auxiliary winding currents. This results in a smooth rotating magnetic field.

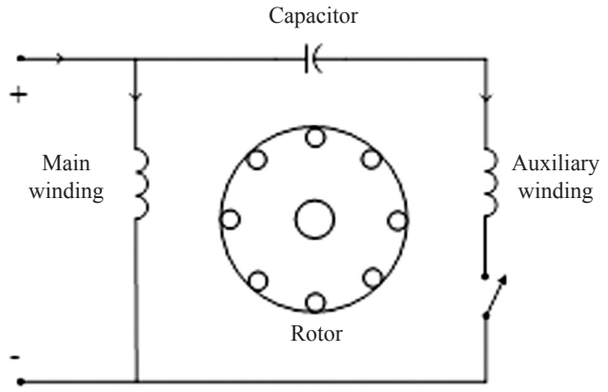

FIGURE 6. Equivalent circuit of a single-phase capacitor start induction motor

In the Figure 6, the main winding is made of thick wire in a much coiled (wrapped) manner and occupies 2/3 of the stator grooves. The auxiliary winding is made of thin wire with less coiling. Rotors of auxiliary windings are usually rotors with squirrel cage (short-circuit rod). In the simulation, many variables must be defined for this main winding, an auxiliary winding, and rotor.

R_s, L_{ls} are stator resistance and leakage inductance for the Main winding of the motor. R_S, L_{lS} are the Auxiliary winding stator resistance and leakage inductance. R'_r, L'_{lr} are rotor resistance and leakage inductance for Main winding of the motor. R'_R, L'_{lR} are resistance of rotor and leakage of inductance for the auxiliary winding of the motor. These two values are equal to the rotor resistance and leakage inductance values of the main winding in the motor respectively. L_{ms} is magnetizing inductance for the main winding of the motor. L_{mS} is magnetizing of the inductance for the auxiliary winding of the motor. L_{ss}, L'_{rr} are stator and rotor inductances of total main winding. L_{SS}, L'_{RR} are stator and rotor inductances for the total auxiliary winding at Henry. V_{as} , i_{as} are stator voltage and current of motor main winding. V_{bs} , i_{bs} are the stator voltage and current of motor auxiliary winding. V_{qs}, i_{qs} are stator voltage and current of the motor at the q-axis. V'_{qr}, $i'qr$ are rotor voltage and current at the q-axis. V_{ds}, i_{ds} are stator voltage and current for d-axis. V'_{dr}, $i'dr$ are rotor voltage and current of d-axis. ϕ_{qs}, ϕ_{ds} are q-d axis fluxes of the stator at pu. ϕ'_{qr}, ϕ'_{dr} are q and d axis fluxes for the rotor at pu. ωm is Angular velocity of the rotor at rad/s. Θ_m is rotor angular position of the motor. p is number of pole pair for motor. ωr is velocity for the electrical angular (ω_m * p) at rad/s. Θ_r is angular position of electrical rotor of the motor at rad/s. Te is Electromagnetic torque of the motor at N*m. Tm is mechanical torque of the shaft as N*m. J is combined rotor and loads inertia coefficient in (kg*m^2). H is combination of the rotor of the motor and load inertia constant of the motor in (s). Partial inductor welds can be added to the motor windings in series and can be added to the general motor equations. L3 = L2 = $L_{SR\ are}$ inductors for source. The equivalent circuit in the d-q axis according to the main winding and auxiliary winding variables of the single-phase asynchronous motor are shown in Figure 7.

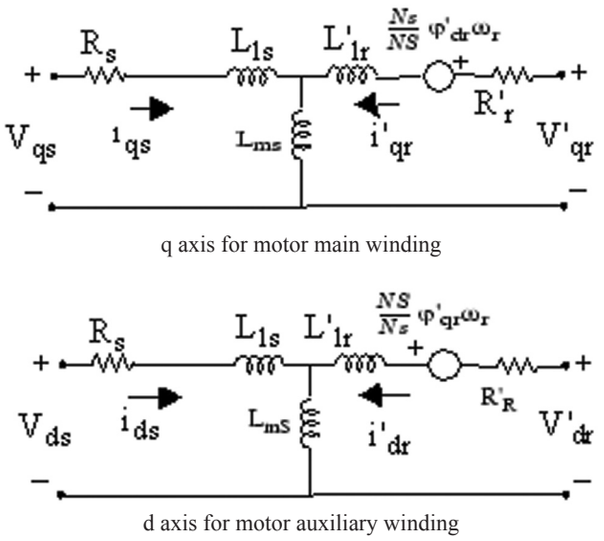

FIGURE 7. The equivalent circuit in the d-q axis according to the main winding and auxiliary winding variables

Equations from equality from 7 to 22 are given for mathematical model of asynchronous motor used in simulation study. Simulations are performed on these models. The equations of the motor structure can be given so, according to d-q axis as in below equations.

$$V_{qs} = d\varphi_{qs}/dt + R_s i_{qs} \quad (7)$$

$$V_{ds} = d\varphi_{ds}/dt + R_S i_d \quad (8)$$

$$V'_{qr} = d\varphi'_{qr}/dt + R'_r i'_{qr} - (N_s/N_S).\omega_r \varphi'_{dr} \quad (9)$$

$$V'_{dr} = d\varphi'_{dr}/dt + R'_R i'_{dr} + (N_S/N_s).\omega_r \varphi'_{qr} \quad (10)$$

$$T_e = p.[(N_S/N_s).\varphi'_{qr} i'_{dr} - (N_s/N_S).\varphi'_{dr} i'_{qr}] \quad (11)$$

$$\varphi_{qs} = L_{ss} i_{qs} + L_{ms} i'_{qr} + L_{sr} i_{qs} \quad (12)$$

$$\varphi_{ds} = L_{SS} i_{ds} + L_{mS} i'_{dr} + L_{sr} i_{ds} \quad (13)$$

$$\varphi'_{qr} = L_{ms} i_{qs} + L'_r i'_{qr} \quad (14)$$

$$\varphi'_{dr} = L_{mS} i_{ds} + L'_{RR} i'_{dr} \quad (15)$$

$$L_{ss} = L_{ms} + L_{ls} \quad (16)$$

$$L_{SS} = L_{lS} + L'_{RR} - L'_{lR} \quad (17)$$

$$L_{ms} = L'_{rr} - L'_{lr} \quad (18)$$

$$L'_{lR} = L'_{RR} - L_{mS} \quad (19)$$

The extra voltage gain (V_{sg}) of the source inductors is in Eq. 20.

$$V_{gs} = L_{sr} i_{ds} = L_{sr} i_{qs} \quad (20)$$

When the extra voltage gain (Vsg) of the source inductors is placed in equality 13 and in equality 14; equality 21 and equality 22 can be achieved.

$$\varphi_{qs} = L_{ss} i_{qs} + L_{ms} i'_{qr} + V_{sg} \quad (21)$$

$$\varphi_{ds} = L_{SS} i_{ds} + L_{mS} i'_{dr} + V_{sg} \quad (22)$$

While the source inductors of the inverter do not work, the vector representation of the resulting stator voltage is given in Figure 8.

While the source inductors of the inverter work, the vector representation of the resulting stator voltage is given in Figure 9.

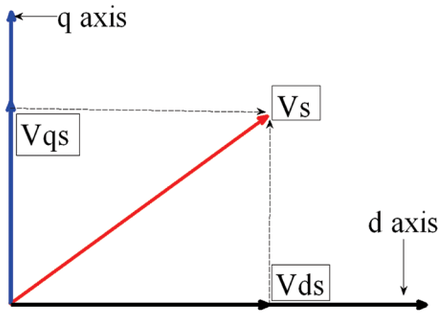

FIGURE 8. Vector representation of the stator voltage without the source inductors

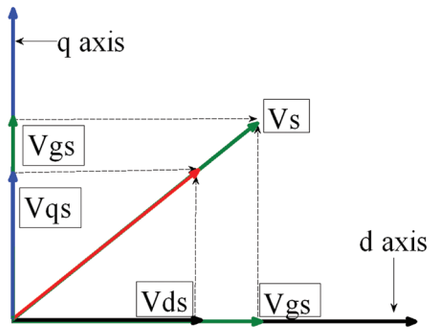

FIGURE 9. Vector representation of the stator voltage without the source inductors

If the inductor sources are not operated, the overall stator voltage is as shown in Figure 8. However, when the source inductors are switched on in the proposed inverter structure, the inverter generates multi-level voltage and also contributes to the voltage generated in the motor windings. The motor winding voltage in the proposed inverter structure can be represented as shown in Figure 9, while the voltage generated in the motor windings of known inverter operations can be represented by the vector representation in Figure 8. So, This is achieved in this study, although this is not achieved in other inverter operations (Vijeh et al. 2019; Buso et al. 2019; Ho et al. 2019; Ramezani et al. 2019; Khajehoddin et al. 2019).

SIMULATION STUDY AND RESULTS

When DC voltage sources are 40 volts, L2 = L3 = 10 micro Henry, R ohm, L = 0.01Henry, the switching frequency of 1 MHz are selected for the inverter circuit in Figure 10, an alternating voltage of 50 Hz is produced as in Fig. 10. Load of Inverter is RLC. R is 0.3ohm, L is 5mH, C is 2mF. Figure 8a shows the generated alternating voltage, while Figure 8b shows the current generated on the load and the harmonic distortion of this current. Figure 8c shows the measurements of the current when the ohmic load in the impedance is changed to 0.2 ohm and 0.5 ohms.

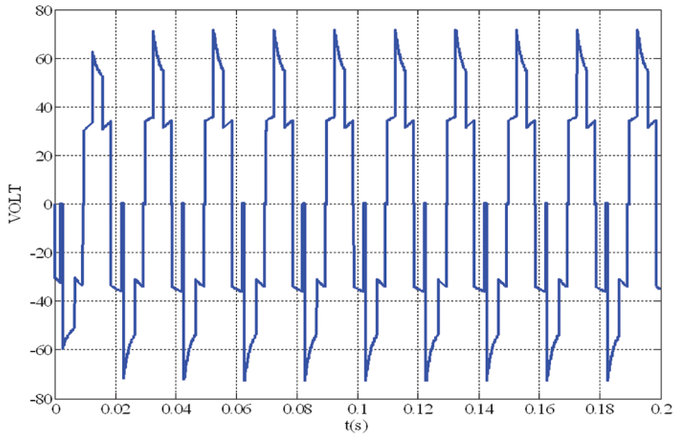

(a)

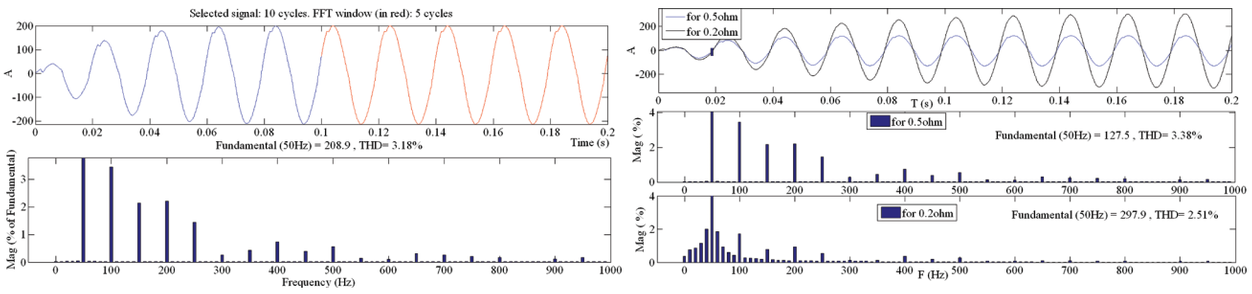

(b) (c)

FIGURE 10. (a) Multi-level voltage generated with DC 50-volt and 10 micro-Henry-split sources (b) harmonic distortion and curent generated with DC 55-volt and 10 micro-Henry-split sources (c) currents and harmonic distortions for impedance including 0.5 ohm and 0.2 ohm

As shown in Figure 10, an alternating voltage of 72 V is obtained from a fixed 55 V of DC source. 55 V of the voltage is increased with 10 microHenry of partial sources to 72 V of voltage at center of the alternating voltage. The current on the RLC load is 208.9 A. The harmonic distortion of this current is 3.18%. This distortion value is less than 5%, which is the IEEE disclosure. The alternating current produced is therefore within the quality standards and is acceptable. In Figure 8c, when the ohmic value in the impedance made to 0.5 ohms, the current is 127.5A while the total value of the harmonic distortion is 3.38%. In Figure 8c, the current is 297.9A while the total value of the harmonic distortion is % 2.51 with the ohmic value in the impedance changing to 0.2 ohm. These values are an acceptable value according to the international standards of IEEE. In the simulation, an alternating voltage of 50 Hz is produced as in Figure 11 when the inductor values of the split source of the inverter are changed by L2 = L3 = 50 micro Henry. For by L2 = L3 = 50 micro Henry, the Figure 11a shows the generated alternating voltage, while Figure 11b shows the current generated on the load and the harmonic distortion of this current.

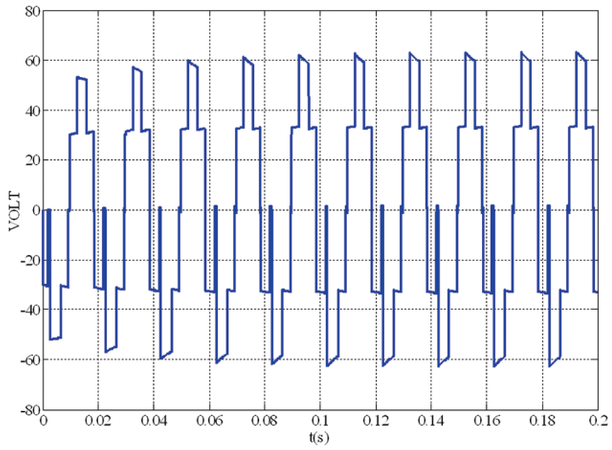

(a)

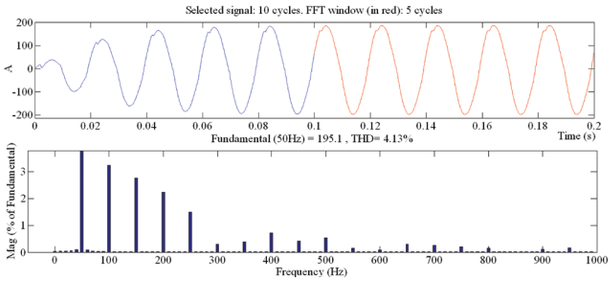

(b)

FIGURE 11. (a) Multi-level voltage generated with DC 55-volt and 50 micro-Henry-split sources (b) harmonic distortion and current generated with DC 50-volt and 50 micro-Henry-split sources

As shown in Figure 11, an alternating voltage of 64 volts is obtained from the fixed DC 55-volt sources. 55 V of the voltage is increased with 10 microHenry of partial sources to 64V of voltage at center of the alternating voltage. The current on the RLC load is 195.1A. The harmonic distortion of this current is 4.13%. This distortion value is less than 5%, which is the IEEE disclosure. While the source inductors are 50 microHenry, the ohmic values in the impedance are changed to 0.2 ohms and 0.5 ohms.

The load current and harmonic distortions for these values are given in Figure 12.

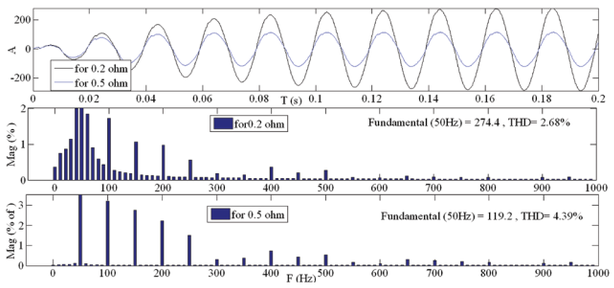

FIGURE 12. Harmonic distortion and current generated with DC 50-volt and 50 micro-Henry-split sources while changing ohm values from 0.2 ohm to 0.5 ohm

When the ohmic value of the impedance is 0.2 ohm, the current on the load is 274.4A and the distortion value is 2.68%. While the ohmic value of the impedance is 0.5 ohm, the current on the load is 119.2A and the distortion value is 4.39%. These degradation values are within international standards. The alternating current produced is therefore within the quality standards and is acceptable.

The resulting currents are in the sinus structure. Therefore, the new inverter structure contributes to this area. Simulation of the single-phase asynchronous motor after simulation of the RLC load is performed as shown in Figure 13. 11 IGBTs are used in the inverter for motor simulation. The source inductor value is 2×10^{-5} H. The four sources used in the circuit are 90V.

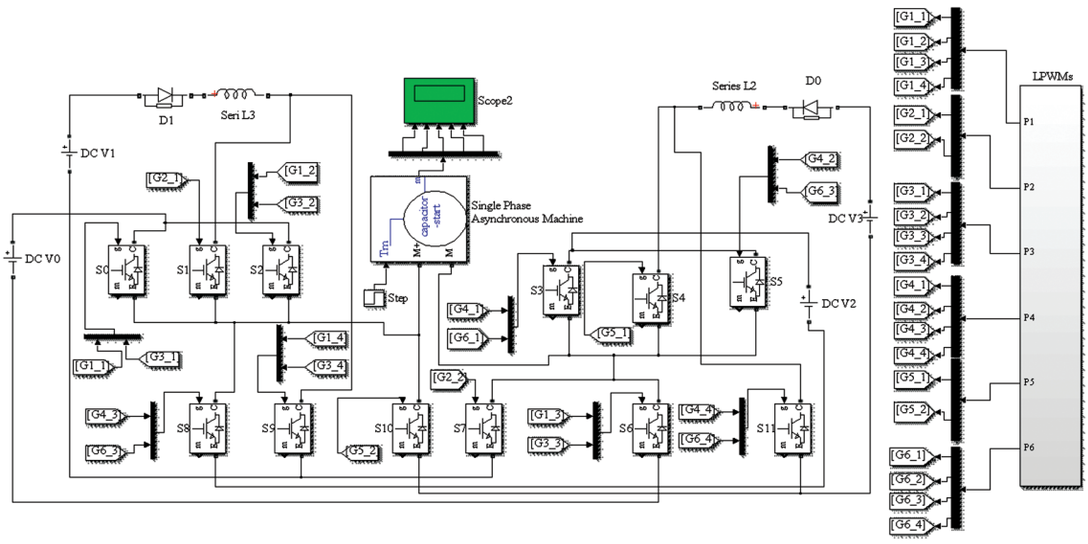

FIGURE 13. Multi-level voltage with DC 40-volt performing single phase asynchronous motor at the simulation

The single-phase asynchronous motor in figure 10 has 18400VA of power, 110Vof input voltage, 60Hz of frequency. $R_s = 2$ ohm, $L_{ls} = 7.2.10^{-3}$H, $R_r' = 4.11$ohm, $L_{lr}' = 5.6.10^{-3}$H, $L_{ms} = 0.18$ H, $R_S = 7.15$ohm, $L_{lS} = 8.54*10^{-3}$, J = 0.015 kg*m^2, p = 1.18 NS/Ns. The six parts LPWM in Figure 1b are distributed to the switches as shown in Figure 11 for the motor test.

The first PWM addressed to G1_4 from G1_1 in order to operate the switches of S0, S2, S6, S9. The second PWM addressed to G2_1 from G2_2 in order to operate the switches of S1, S7. The third PWM addressed to G3_1 from G3_4 in order to operate the switches of S0, S2, S6, and S9. The fourth PWM addressed to G4_1 from G4_4 in order to operate the switches of S3, S5, S8, S11. The fifth PWM addressed to G5_1 from G5_2 in order to operate the switches of S4, S10. The sixth PWM addressed to G6_1 from G6_4 in order to operate the switches ofS3, S5, S8, and S11.

Figure 14 shows forming of the alternating voltage at the 50 Hz of frequency on the motor when the induction motor is running at Matlab Simulink.

Performance measurements of the engine are given in 3s. However, since the multi-level voltage is not fully visible at 3s, the voltage value at 0.2s is given in Figure 9.The DC 90V applied to the inverter is transformed to 120 volt alternating voltage on the motor as shown in Figure 14. The 90V DC source is converted to an alternating voltage of 120 V on the load without the use of an extra circuit such as dc-dc converter. Figure 15 shows the current change at the main and auxiliary windings of the motor.

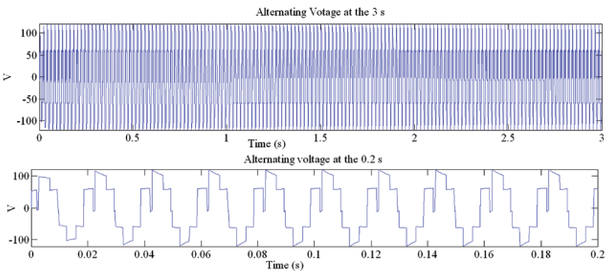

FIGURE 14. The alternating voltage at the 50 Hz of frequency on the motor

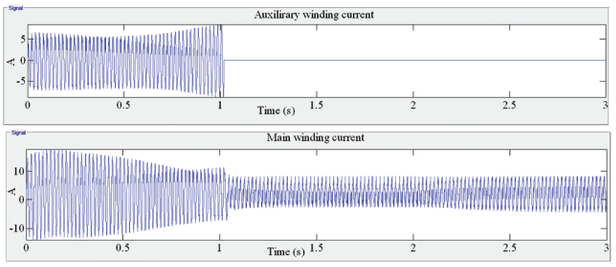

FIGURE 15. The current change in the main winding and auxiliary windings of the motor

The currents of the main winding and auxiliary windings of the motor is stable at the 1s. The 10A of current at the motor main winding is the maximum value, while 20A of the current auxiliary windings is the maximum value. Figure 16

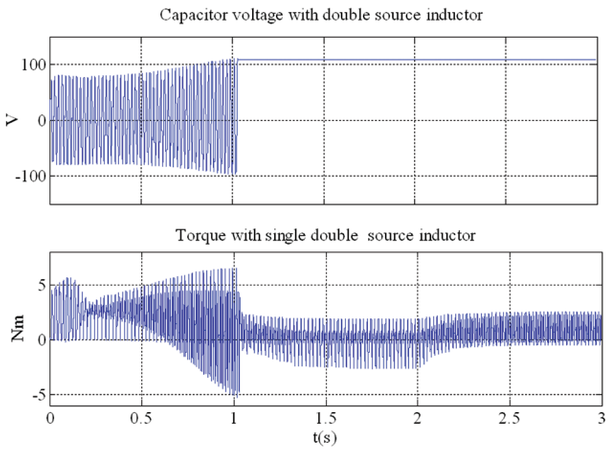

FIGURE 16. The capacitor voltage change and electromotor change of the motor

demonstrates the capacitor voltage change and electromotor change of the motor.

Voltage of the capacitor and electromagnetic torque at the motor are stable at the 1s. The 10 Nm of electromagnetic torque of the motor is the maximum value, while 120V of the capacitor voltage is the maximum value. Figure 17 shows the rotor speed.

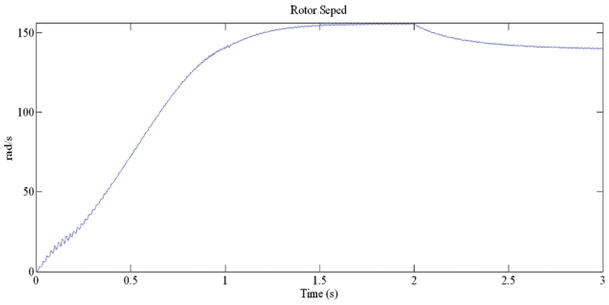

FIGURE 17. The rotor speed of motor

The speed of the engine reaches 160 rad / s at 1.5 s. the motor achieves this with a DC voltage source of 90 V via the inverter method. If the motor is operated with a single-sided source inductor, the capacitor voltage and electro-magnetic torque become as shown in Figure 18.

When the motor is driven by disabling one of the source inductors of the inverter, a unilateral multi-level alternating voltage is generated on the motor. One of the source inductors is not in the circuit, the times of stabilization of the torque and capacitor voltage increase from 1s to 1.5s. When the motor is operated with a single-sided source inductor, the main and auxiliary windings of the motor become as shown in Figure 19.

One of the source inductors is not in the circuit, the times of stabilization of the main and auxiliary windings of the motor increase from 1s to 1.5s. After inverter with a single-sided source inductor runs the motor, rotor speed of the motor becomes in Figure 20.

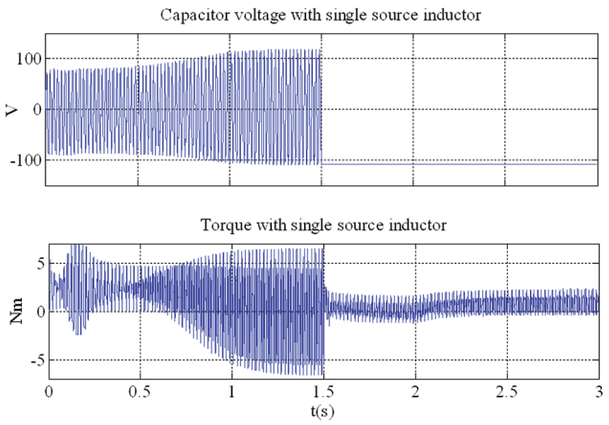

FIGURE 18. The capacitor voltage and electro-magnetic torque for inverter with a single-sided source

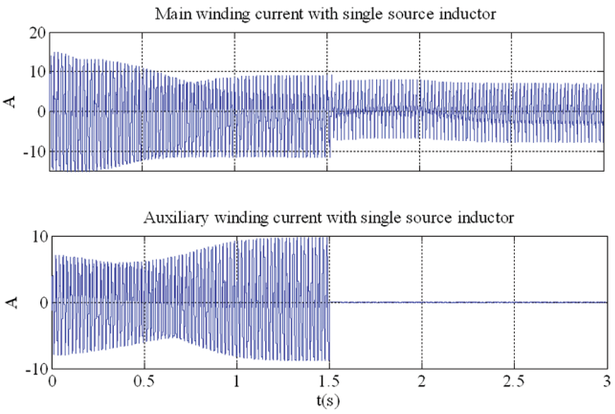

FIGURE 19. The main and auxiliary windings of the motor for inverter with a single-sided source

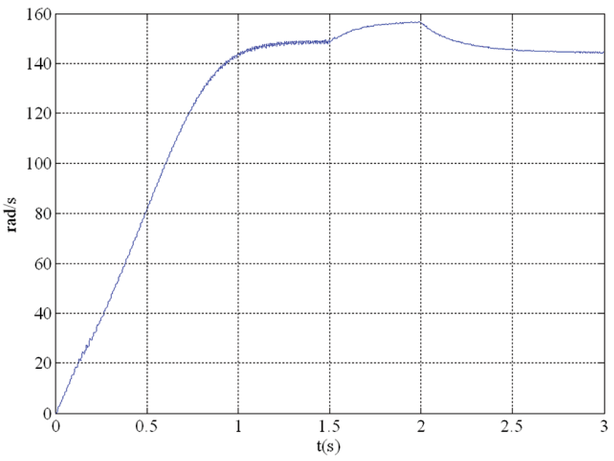

FIGURE 20. Rotor speed of inverter with a single-sided source inductor running the motor

After the rotor speed reaches 150 rad/s at 1.5 s, the rotor speed reaches 158 rad/at the 2 s. At 2.5 s, 150 rad/s is also stable. These observed values indicate the effect of split source inductors and the split source approach on the

circuit. While conventional inverters generate multiple levels, they cannot generate a voltage level more than the level of constant input sources. So, the input voltage source value that is available determines the maximum value of the generated multilevel voltage. If resources at the same level have to be used, this recommended system provides higher a voltage at the loads than a voltage value of the source while generating the multiple levels. The motor can be operated for the full performance although maximum value of the constant voltage source is insufficient to feed the motor.

CONCLUSION

In this study, the performance of the single-phase multi-level inverter with partial inductor source was presented. The operation of the circuit elements was given by describing the operation of the circuit according to four different circuit conditions for six parts time. Simulation of the circuit with the working principle described was done in Matlab Simulink. Applications of RLC load and the asynchronous motor was performed in the simulation application. While the voltage measurements for the RLC load were performed; measurements of the main wing current, auxiliary wing current, electromagnetic torque, and rotor speed were made on the asynchronous motor. After the simulation applications, while the10 mH of inductors were connected to the input DC voltage sources of the inverter, Current and voltage values on the load were measured. The current on the RLC load was 208.9 A. The harmonic distortion of this current is 3.18%. This distortion value was less than 5%, which is the standard of IEEE. The alternating current produced was therefore within the quality standards and was acceptable.

After that, while the 10 mH of inductors was connected to the input DC voltage sources of the inverter, Current and voltage values on the load were measured. The current on the RLC load was 195.1 A.

The harmonic distortion of this current is 4.13%. This distortion value was less than 5%, which is the IEEE disclosure. The alternating current produced was therefore within the quality standards and is acceptable. After the asynchronous motor simulation, the main winding current and the auxiliary winding current of the motor were stabilized at 1s. The capacitor voltage and motor torque were also stable at 1s. For knowing the effect of the inductor on the circuit; the inverter was tested a unilateral inductor source while the motor was driven. For the engine performance, it is seen that the obtained speed, torque, main and auxiliary winding current values were impaired while their settling time is increasing from 1s to 1.5s. This showed the effect of the fragmented source in the proposed system. But, if resources at the same level were available to be used, this recommended system provided a higher voltage than a voltage value of the source for the loads while generating the multiple levels. The measured values of the asynchronous motor have shown that these values can reach sufficient values for the motor in a short time period. These results showed that this study successfully was designed and implemented with a new circuit structure.

REFERENCES

Ahmadi, R., Mahmoudi, H. & Aleenejad, M. 2019. Torque ripple minimization for a permanent magnet synchronous motor using a modified quasi-z-source inverter. *IEEE Transactions on Power Electronics* 34(4): 3819-3830.

Ananda, A.S. 2018. *Performance analysis of series-passive filter in 5-phase PWM inverter drive and harmonic study using Simulink/Matlab.* Advances in Power Systems and Energy Management. Springer, Singapore.

Babae, E., Suryawanshi, H.M. & Abu-Rub, H. 2018. Z-source converters: Topologies, modulation techniques, and applications–Part II. *IEEE Transactions on Industrial Electronics* 65(10): 8274-8276.

Bauer, J. 2010. Single phase voltage source inverter photovoltaic application. *Acta Polytechnica* 50(4): 7-11.

Buso, S., Caldognetto, T. & Liu, Q. 2019. Analysis and experimental characterization of a large-bandwidth triple-loop controller for grid-tied inverters. *IEEE Transactions on Power Electronics* 34(2): 1936-1949.

Can, E. & Sayan, H.H. 2016. SSPWM three phase inverter design and experimented on unbalanced loads. *Tehnički vjesnik* 23(5): 1239-1244.

Cavalcanti, M.C., Bradaschia, F., de-Melo, N.M.T., Azevedo, G.M.S. & Cardoso, T.D. 2018. Dynamic modeling and control system design of the buck-boost-based three-state three-phase Z-source inverter. *International Journal of Electrical Power & Energy Systems* 104: 654-663.

Ho, D., Vegiraju, S., Choi, D., Cho, C.H., Kwon, G., Huang, P.C., Lee, G.H., Earmme, T., Yau, S.L., Chen, M.C. & Kim, C. 2019. Solution-processable small molecules for bulk heterojunction ambipolar thin-film transistors and complementary-like inverters. *Dyes and Pigments* 163: 725-733.

Huang, Y., Xu, Y., Zhang, W. & Zou, J. 2018. PWM frequency noise cancellation in dual three-phase motor using parallel interleaved inverters. *IEEE Transactions on Power Electronics*, 1-7.

Kerem, A., Aksoz, A., Saygin, A., Yilmaz, E. N. 2017. Smart grid integration of micro hybrid power system using 6-switched 3- level inverter. *Smart Grid and Cities Congress and Fair (ICSG) International Istanbul*, 161-165.

Khajehoddin, S.A., Karimi-Ghartemani, M. & Ebrahimi, M. 2019. Grid-Supporting Inverters With Improved Dynamics. *IEEE Transactions on Industrial Electronics* 66(5): 3655-3667.

Kim, M. & Balog, R.S. 2018. THD analysis for a high frequency link SCR-based PWM inverter. *Texas Power and Energy Conference (TPEC)*, 256: 1-6.

Kumar, M. 2018. Time-domain characterization of digitized pwm inverter with dead-time effect. *IEEE Transactions on Circuits and Systems I: Regular Papers*, 99: 1-10.

Madhu, S.B.G., Narayana, V.R. & Priya, N.D. 2018. A comparison of seven-level inverter topologies with minimum number of switches for induction motor drive. *International Journal of Engineering Science* 8(4): 17332-17336.

Nguyen, G., Odawara, S., Endo, T., Taki, C., Fujisaki, K., Iwamoto, F., Yamada, T. & Sasaya, T. 2018. Motor core losses evaluation with PWM and PAM inverter excitations in computational analysis and experiments. *2018 IEEE International Magnetic Conference (INTERMAG)* 87: 1-2.

Özbay, H., Öncü, S. & Kesler, M. 2017. SMC-DPC based active and reactive power control of grid-tied three phase inverter for PV systems. *International Journal of Hydrogen Energy* 42(28): 17713-17722.

Paterakis, F.K., Nafpaktitis, D., Darwish, M. & Grigorios, K.E. 2018. A modified algorithm based on the equal-areas PWM for the extend of linear operation of a microprocessor-controlled PWM-VSI. *International Journal of Robotics and Mechatronics* 5(1): 12-19.

Rajesh, B. 2018. Three-level flying capacitor multilevel inverter is used to suppress harmonics at the output of 3-phase inverter drive and study of heat at various parts of 3-phase induction motor. Advances in Systems, Control and Automation. Slide.

Ramezani, M., Li, S., Musavi, F. & Golestan, S. 2019. Seamless transition of synchronous inverters using synchronizing virtual torque and flux linkage. *IEEE Transactions on Industrial Electronics* 1-1: 1-10.

Reddy, K., Raghava, M. & Kumar, M.V. 2017. Simulation of H6 full bridge Inverter for grid connected PV system using SPWM technique. *International Research Journal of Engineering and Technology* 4(1): 1452-1457.

Singh, S.N. & Singh, G.K. 2017. Modeling, design and stability analysis of an improved SEPIC converter for renewable energy systems. *International Journal of Electronics* 104(9): 1527-1545.

Singh, G., Kumar, T.C.A. & Naikan, V.N.A. 2018. A nonintrusive methodology for bearing current detection in PWM inverter fed induction motor drive. *2018 International Conference on Power, Instrumentation, Control and Computing (PICC)*, 1-6.

Viana, A.G. & Ramos, D.S. 2018. Outcomes from the first large-scale solar PV auction in Brazil. *Renewable and Sustainable Energy Reviews* 91: 219-228.

Vijeh, M., Rezanejad, M., Samadaei, E. & Bertilsson, K. 2019. A general review of multilevel inverters based on main submodules: structural point of view. *IEEE Transactions on Power Electronics* 34(10): 9479-9502.

Yao, A., Odawara, S. & Fujisaki, K. 2018. Iron loss and hysteretic properties under pwm inverter excitation at high ambient temperatures. *IEEJ Journal of Industry Applications* 7(4): 298-304.

Yusof, Y. & Rahim, A.N. 2011. Comparative study between spwm control techniques THIPWM for PWM-VSI using mathematical modeling and simulation. *Jurnal Kejuruteraan* 23: 17-26.